Fermi National Accelerator Laboratory

FERMILAB-Pub-78/43-EXP
7420.180

(Submitted to Phys. Rev. D)

INCLUSIVE NEGATIVE HADRON PRODUCTION FROM HIGH ENERGY $\bar{\nu}$ NUCLEUS CHARGED-CURRENT INTERACTIONS

J. P. Berge, D. Bogert, R. Endorf, R. Hanft, J. A. Malko,
G. Moffatt, F. A. Nezrick, W. Scott, W. Smart,
and J. Wolfson
Fermi National Accelerator Laboratory
Batavia, Illinois 60510 USA

and

V. V. Ammosov, A. H. Amrakhov, A. G. Denisov, P. F. Ermolov,
V. A. Gapienko, V. I. Klukhin, V. I. Koreshev,
P. V. Pitukhin, V. G. Rjabov, E. A. Slobodyuk, and
V. I. Sirotenko
Institute of High Energy Physics
Serpukhov, USSR

and

V. I. Efremenko, P. A. Gorichev, V. S. Kaftanov,
V. D. Khovansky, G. K. Kliger, V. Z. Kolganov, S. P. Krutchinin,
M. A. Kubantsev, A. N. Rosanov, M. M. Savitsky, and
V. G. Shevchenko
Institute of Theoretical and Experimental Physics
Moscow, USSR

and

C. T. Coffin, R. N. Diamond, H. French, W. Louis, B. P. Roe,
R. T. Ross, A. A. Seidl, and D. Sinclair
University of Michigan
Ann Arbor, Michigan 48109 USA

May 1978

INCLUSIVE NEGATIVE HADRON PRODUCTION FROM HIGH ENERGY $\bar{\nu}$ NUCLEUS CHARGED-CURRENT INTERACTIONS*

J. P. Berge, D. Bogert, R. Endorf,[a] R. Hanft,[b] J. A. Malko, G. Moffatt,[a] F. A. Nezrick, W. Scott, W. Smart, and J. Wolfson
Fermi National Accelerator Laboratory
Batavia, Illinois 60510 USA

and

V. V. Ammosov, A. H. Amrakhov, A. G. Denisov, P. F. Ermolov, V. A. Gapienko, V. I. Klukhin, V. I. Koreshev, P. V. Pitukhin, V. G. Rjabov, E. A. Slobodyuk, and V. I. Sirotenko
Institute of High Energy Physics
Serpukhov, USSR

and

V. I. Efremenko, P. A. Gorichev, V. S. Kaftanov, V. D. Khovansky, G. K. Kliger, V. Z. Kolganov, S. P. Krutchinin, M. A. Kubantsev, A. N. Rosanov, M. M. Savitsky, and V. G. Shevchenko
Institute of Theoretical and Experimental Physics
Moscow, USSR

and

C. T. Coffin, R. N. Diamond,[c] H. French,[d] W. Louis, B. P. Roe, R. T. Ross, A. A. Seidl, and D. Sinclair
University of Michigan
Ann Arbor, Michigan 48109 USA

*Work supported in part by the U.S. Department of Energy and the National Science Foundation.

[a]Visitor from: University of Cincinnati, Cincinnati, Ohio 45221.

[b]Present address: CERN, 1211 Geneva 23, Switzerland.

[c]Present address: Florida State University, Tallahassee, Florida 32306

[d]Present address: Columbia University, New York, New York 10027.

ABSTRACT

We present data on inclusive negative hadron production from charged current antineutrino interactions in a 21% Ne-H mixture. Inclusive single particle distributions are presented and are shown to be insensitive to the momentum transferred to the hadron vertex. Comparisons made to inclusive data from π^-p and π^-n interactions indicate a close similarity between the hadrons resulting from π-nucleon and $\bar{\nu}$-nucleus interactions. The general features of the $\bar{\nu}$-nucleus data are found to be similar to those seen in $\bar{\nu}p$ interactions. This last observation implies that $\bar{\nu}p$ and $\bar{\nu}n$ interacions are similar and that neuclear effects are small.

I. INTRODUCTION

Measurements of inclusive hadron production in neutrino and antineutrino induced reactions play a crucial role in our understanding of hadron production in a large class of related processes. In this paper we report on a study of inclusive negative hadron production by antineutrinos, carried out using the Fermilab 15-Ft. bubble chamber filled with a 21% atomic neon-hydrogen mixture. With this mixture 16% of the interactions are off of free hydrogen targets.

Muon inclusive distributions (x and y distributions) for the reaction $\bar{\nu}_\mu$ + Nucl → μ^+ + hadrons as measured in this experiment are published in a separate paper.[1] The data were based on approximately 600 events in the energy range 10-200 GeV. The data presented here are based on the same event sample and the procedures and criteria employed in the analysis are identical: events are included in the sample if they have a positive muon, identified by the EMI,[2] with momentum greater than 4 GeV/c and if the energy transfer to the hadrons measured in the lab is greater than 2.0 GeV.

In this experiment it is in general not possible to make an unambiguous mass assignment for the charged hadrons except at very low momentum (< 1 GeV/c). For the negative tracks the majority (> 90%) are pions and for this analysis all negative tracks have been assigned a pion mass. The positive tracks include some unidentified protons which could obscure the interpretation of the results if they were systematically assigned

the wrong mass hypothesis. For this reason distributions for positive hadrons are not shown.

II. EXPERIMENTAL RESULTS

We have analyzed the inclusive negative hadron (h^-) production in terms of the variables W^2, Q^2, p_t^2, P_{out}^2, $Z = E_{(h^-)}/E_{Had}$ and $X_F = 2\ P_{||}^*/W$. Here W is the total hadronic energy, P_t and $P_{||}^*$ are the transverse and longitudinal h^- momentum respectively, all calculated in the hadronic rest frame; $E_{(h^-)}$ and E_{Had} are the h^- energy and total hadronic energy calculated in the laboratory system; Q^2 is the square of the four-momentum transfer between the $\bar{\nu}$ and μ^+; P_{out} is the h^- momentum perpendicular to the $\bar{\nu}\mu^+$ production plane. The variables X_F, W^2 and p_t^2 so defined are common to inclusive studies using hadron beams.

Figures 1(a) and (b) show respectively the W^2 and Q^2 distributions for our data sample. We note that although W^2 goes out to values greater than 80 GeV^2, the average W^2 is much lower, being approximately 15 GeV^2. (For a pion-nucleon interaction this W^2 corresponds to an ~8 GeV/c incident pion momentum). Thus, in terms of the hadronic energy, these data are in a comparitively low energy region.

Figure 2(a) shows the average h^- multiplicity as a function of $\ln W^2$. The data appear to be linear in $\ln W^2$; the solid line in Fig. 2(a) is the result of a fit to a linear form $A + B\ln W^2$ and yields $\langle h^- \rangle = (-0.25 \pm .03) + (0.76 \pm 0.01) \ln W^2$ in the

$4 < W^2 < 100$ GeV^2 region ($\chi^2/ND = 4.2/10$). This linear behavior is not significantly dependent on Q^2. Fits to the same linear form yield parameters A = -0.17 ± 0.18, B = 0.69 ± 0.09 in the region $Q^2 < 2$ (GeV/c)^2 and A = -0.05 ± 0.19, B = 0.71 ± 0.08 in the region $2 < Q^2 < 10$ (GeV/c)^2. For comparison the triangles in Fig. 2(a) show the $< h^- >$ distribution obtained from $\bar{\nu}p$ interactions.[3] Since the weak current transfers a negative charge to the target nucleon we have compared our data in Fig. 2(a) to data obtained from π^-p interactions (dashed curve).[4] We note that the $< h^- >$ distributions for both the $\bar{\nu}p$ and π^-p data appear to be slightly lower than the $\bar{\nu}$ nucleus data. This may be explained in part by the fact that in the $\bar{\nu}$ nucleus data there are both neutron and proton targets, and the $< h^- >$ multiplicity is somewhat higher for a neutron target.[5]

In contrast to the observed dependence of $< h^- >$ on W^2, we see in figures 2(b)-2(d) that $< h^- >$ is weakly dependent on Q^2 with only a possible small dependence in the low W^2 region. This small Q^2 dependence is in agreement with results obtained from $\bar{\nu}p$ data.[3]

In figures 3(a) and (b) are presented the normalized Z distributions for two W^2 and two Q^2 regions respectively. In the quark parton model high-Z particles are fragments from one quark only and are predicted to be independent of Q^2 and W^2. The distributions in Fig. 3 are consistent with this interpretation, although the onset of this scaling behavior at such small Z values is probably fortuitous.

The dependence of $< P_t >$ on Q^2, W^2 and Z is shown in figures 4(a), (b) and (c) respectively. We see that $< P_t >$ is independent of Q^2. This independence has been seen previously in $\bar{\nu}$, ν and e scattering.[3,6,7] The distribution of $< P_t >$ vs. W^2 (Fig. 4(b)) exhibits a slow rise with increasing W^2 and perhaps a plateau at high W^2. The distribution of $< P_t >$ vs. Z (Fig. 4(c)) rises with increasing Z, the dependence appearing to be approximately linear in $\ell n(Z)$. We present in figures 4(d), (e) and (f) the distributions of $< P_{out} >$ as a function of Q^2, W^2 and Z. The $< P_{out} >$ distributions have the same qualitative dependences as those for $< P_t >$. The $< P_t >$ distributions of Fig. 4 are in general agreement with results from inclusive $\bar{\nu}p$ data[3] and inclusive hadron data. We note however that the $\bar{\nu}p$ data appear to show the onset of a plateau in $< P_t >$ vs. Z at $Z \simeq 0.3$ which is not indicated by the data in Fig. 4(c). Although the errors are large, Fig. 4(c) is consistent with $< P_t >$ being independent of W^2 in the high Z region.

Figure 5 shows the p_t^2 distribution of the inclusive h^- sample for all the data and for the subsamples having $4 < W^2 < 20$ GeV^2 and $20 < W^2 < 100$ GeV^2. We have fit these distributions in the range $0.0 \leq P_t^2 < 1.0$ (GeV/c)^2 to the form $dN/dp_t^2 = Ae^{-Bp_t}$, obtaining B values of $(6.54 \pm .20)$ (GeV/c)$^{-1}$ (χ^2/ND = 8.4/5) and $(5.81 \pm .40)$ (GeV/c)$^{-1}$ (χ^2/ND = 1.9/5) for $4 < W^2 < 20$ GeV^2 and $20 < W^2 < 100$ GeV^2 respectively. We note that the data in general give poorer fits[8] to the form $dN/dp_t^2 = Ae^{-Bp_t^2}$.

This latter form was used to parameterize the inclusive hadronic distributions in the $\bar{\nu}p$ data of Ref. 3.

To study the Feynman scaling behavior of the inclusive h^- data we define the invariant structure function $f_1(X_F)$ by

$$f_1(X_F) = \frac{1}{N_{tot}} \int \frac{E^*}{\sqrt{W^2}} \frac{d^2n}{dX_F dp_t^2} dp_t^2,$$

where E^* is the h^- energy in the hadron rest frame, N_{tot} is the total number of events and n is the number of h^- tracks. The distributions of f_1 for two W^2 and two Q^2 regions are shown in figures 6(a) and (b) respectively. In the nomenclature of strong interaction physics Feynman scaling manifests itself as the independence of f_1 with respect to the total hadronic energy, W. As seen from Fig. 6(a), the invariant structure function $f_1(X_F)$ shows no strong W^2 dependence when compared between the regions $4 < W^2 < 20$ GeV^2 and $20 < W^2 < 100$ GeV^2. Likewise, the f_1 distributions in Fig. 6(b) show no significant Q^2 dependence. The absence of a strong W^2 dependence for f_1 is perhaps not surprising. The average W^2 for the $4 < W^2 < 20$ GeV^2 and $20 < W^2 < 100$ GeV^2 regions is ~10 and ~35 GeV^2 respectively. In a comparison[9] of $f_1(X)$ between an S of 16 and 35 GeV^2, obtained from π^-p data, it was found that $f_1(X_F)$ varied by less than ~10% in the region $-.6 < X_F < .6$.

In Fig. 7 we have compared our $f_1(X_F)$ distributions with those obtained from other experiments. Figure 7(a) shows the distribution of $f_1(X_F)$ for our total data sample (solid circles)

and the same distribution obtained from the $\bar{\nu}p \to \mu^+ h^- X$ interaction.[3] The two distributions are in excellent agreement over almost the entire X_F range.

In Fig. 7(b) we have replotted the $f_1(X_F)$ distribution for the $20 < W^2 < 100$ GeV^2 region. We have compared this distribution to $\pi^- p$[8] and $\pi^+ p$ data[10] (i.e., charge conjugate of $\pi^- n$) having $s \sim 35$ GeV^2, since this s value corresponds to the average W^2 in the 20-100 GeV^2 region. In the 21% Neon-Hydrogen mixture there are 1.4 proton targets for each neutron. Since the $\bar{\nu}$ interacts off of u-type quarks, we have added the $\pi^- p$ and $\pi^- n$ data with the relative weights $(1.4 \times 2) f_1(\pi^- p) + f_1(\pi^- n)$. The result is shown by the solid curve in Fig. 7(b), where the data have been normalized at $X_F = 0.0$. We note that the hadron data show a characteristic forward peak (leading particle effect) which is not observed in the antineutrino data. Except in the large $|X_F|$ regions the shape of the hadron and antineutrino data are in reasonable agreement.

III. CONCLUSION

We find that in general the overall properties of the inclusive h^- data obtained from $\bar{\nu}$ nucleus interactions are similar to those obtained from inclusive π-nucleon data. In addition the inclusive h^- distributions are found to be insensitive to the momentum transferred to the hadronic vertex. These results imply that in $\bar{\nu}$ interactions the hadronic vertex has only a small

"memory" of the details of the leptonic vertex. In the 21% Ne-H mixture used in this exposure 42% of the target nucleons are neutrons in the Ne nuclei. The similarities observed between the $\bar{\nu}$ interactions in this Ne-H mix and $\bar{\nu}$ interactions in hydrogen imply that $\bar{\nu}p$ and $\bar{\nu}n$ interactions are similar and that nuclear effects in our data are small compared to our statistical errors.

REFERENCES

[1]Fermilab-IHEP-ITEP-Michigan Neutrino Group, Phys. Rev. Lett. 39, 382 (1977).

[2]R. J. Cence et al., Nucl. Instr. Methods, 138, 245 (1976).

[3]M. Derrick et al., Phys. Rev. D17, 1 (1978).

[4]The dashed curve indicates the W^2 dependence of the $< h^- >$ observed in inelastic $\pi^- p$ interactions, where W^2 is defined here as the $\pi^- p$ center of mass energy squared. The following data were used to obtain the curve:
(for $W^2 = 7.47$) M. S. Ainutdinov et al., JETP 20, 69 (1965); A. Citron et al., Phys. Rev. 144, 1101 (1966); M. L. Perl et al., Phys. Rev., 132, 1252 (1963).
(for $W^2 = 19.67$) Bardadin et al., JINR511/6 - 1964 (as referenced in CERN/HERA 72-1); W. Galbraith et al., Phys. Rev. 138, B913 (1965); S. Brandt et al., Phys. Rev. Lett. 10, 413 (1963).
(for $W^2 = 38.43$) G. W. Brandenburg et al., Nucl. Phys. B16, 287 (1970); K. J. Foley et al., Phys. Rev. Lett. 11, 425 (1963); S. P. Denisov et al., Phys. Lett. 36B, 528 (1971).
(for $W^2 = 47.8$) J. W. Elbert et al., Nucl. Phys. B19, 85 (1970); S. P. Denisov et al., Phys. Lett. 36B, 528 (1971).
(for $W^2 = 75.96$) O. Balea et al., Phys. Lett. 39B, 571 (1972).

[5]In a separate analysis of this same $\bar{\nu}$ Nucleus exposure which separated the data in terms of interactions off of neutron and proton targets, it was found that $< h^- > = 2.0 \pm 0.3$ for

the neutron sample and $< h^- > = 1.7 \pm 0.1$ for the proton sample. (see "$\bar{\nu}p$ and $\bar{\nu}n$ Charged Current Interactions Unfolded from $\bar{\nu}$ Neon Events in the 15-Ft. Fermilab Bubble chamber" - J. P. Berge et al., - to be submitted to Phys. Rev. Lett.) We also note that for $P_{inc} = 40$ GeV/c, $< h^- >$ for π^-n interactions is 10% higher than $< h^- >$ for π^-p interactions (see O. Balea et al., Ref. 5).

[6]J. W. Chapman et al., Phys. Rev. D14, 5 (1976).

[7]L. Hand, Talk presented at the 1977 International Symposium on Lepton and Photon Interactions at High Energy, Hamburg, Aug. 25-31, 1977.

[8]When we fit to $dN/dP_t^2 \alpha e^{-BP_t^2}$ we obtain B = (9.50 ± 0.46) $(GeV/c)^{-2}$ ($\chi^2/ND = 34.2$) and B = (7.09 ± 0.53) $(GeV/c)^{-2}$ ($\chi^2/ND = 13.6/5$) in the range $4 \leq W^2 < 20$ GeV^2 and $20 \leq W^2 < 100$ GeV^2 respectively.

[9]W. D. Shepard et al., Phys. Rev. Lett. 27, 1164 (1971).

[10]For $\pi^-n \to \pi^-X$ we used data for $\pi^+p \to \pi^+X$ at 16 GeV/c: Beaupre et al., Phys. Lett. 37B, 432 (1971).

FIGURE CAPTIONS

Figure 1: Distribution of (a) W^2 and (b) Q^2 for the selected $\bar{\nu}$ nucleus charged current events.

Figure 2: Distribution of $< h^- >$ with respect to (a) W^2 and (b), (c) and (d) Q^2, W^2. In (a) comparisons are made with $\bar{\nu}p$ data (triangular points) and $\pi^- p$ data (dashed curve). The solid line is a fit to an $A + B \ell n W^2$ term.

Figure 3: Normalized Z distributions for (a) two Q^2 regions and (b) two W^2 regions .

Figure 4: Distribution of $< P_t >$ with respect to (a) Q^2, (b) W^2 and (c) Z. The same distributions for $< P_{out} >$ (d), (e) and (f).

Figure 5: Distribution of P_t^2 for total data and two W^2 regions.

Figure 6: Distribution of $f_1(X_F)$ for (a) two W^2 regions and (b) two Q^2 regions.

Figure 7: (a) Comparison of $f_1(X_F)$ for $\bar{\nu}$ nucleus interactions (solid data points) and $\bar{\nu}p$ interactions [Reference 3] (open data points). (b) Comparison of $f_1(X_F)$ from $\bar{\nu}$ Nucleus interactions and $\pi^- p$ [Reference 9] plus $\pi^- n$ [Reference 10] interactions.

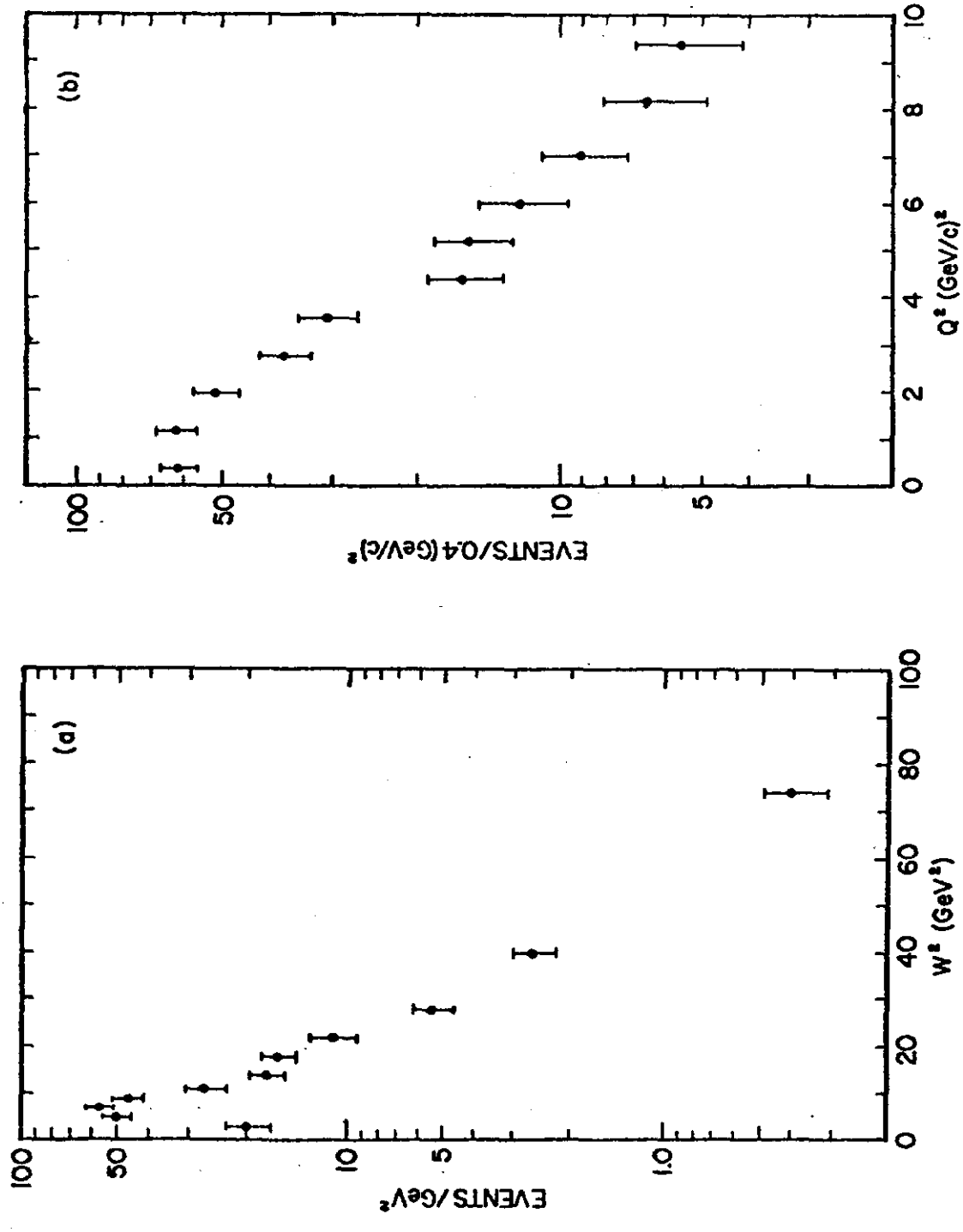
(b)
EVENTS/0.4 (GeV/c)²
100
50
10
5
0
2
4
6
8
10
Q² (GeV/c)²
(a)
EVENTS/GeV²
100
50
10
5
1.0
0
20
40
60
80
100
W² (GeV²)

Figure 1

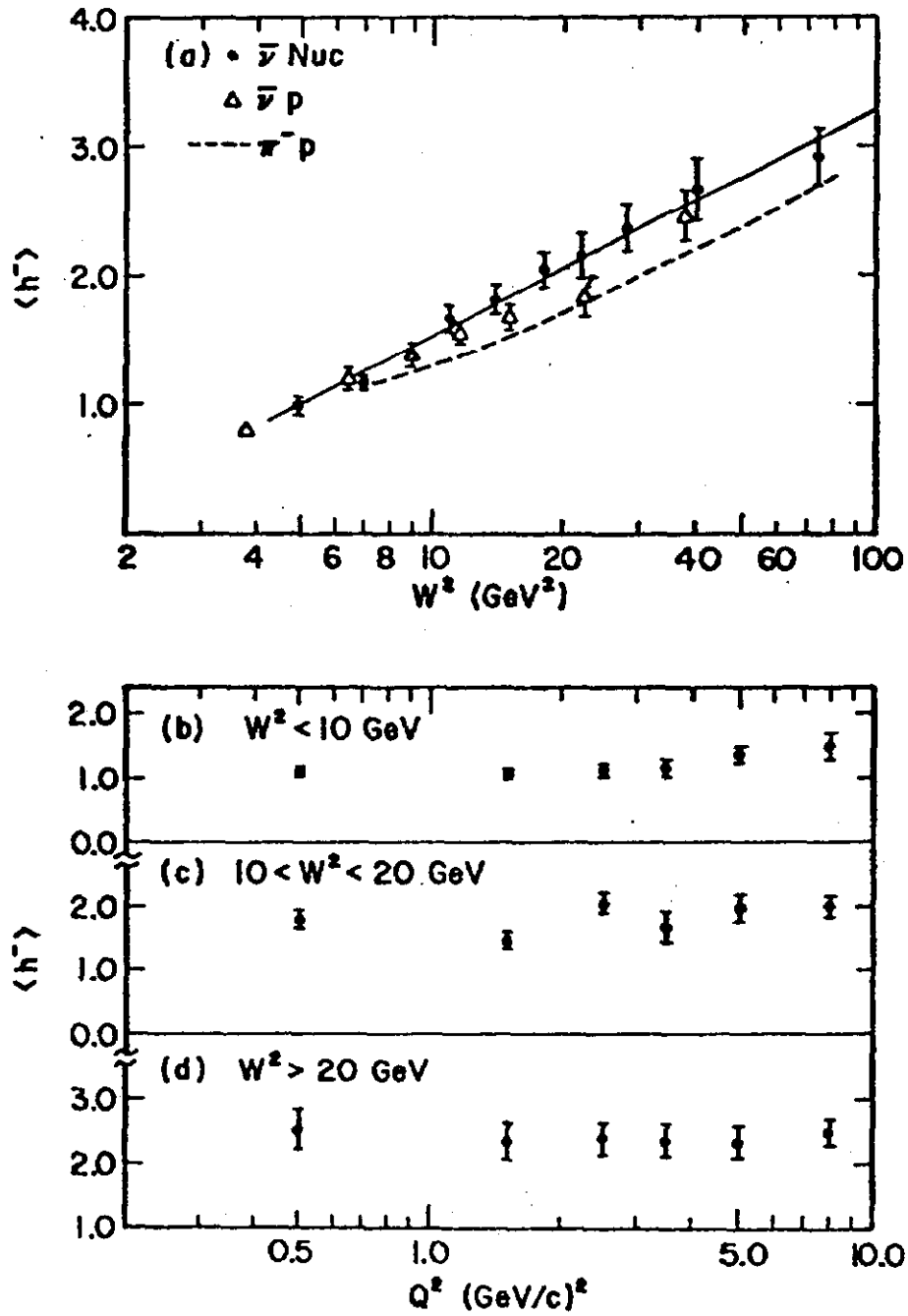
(a) • $\bar{\nu}$ Nuc
△ $\bar{\nu}$ p
---- π^- p
$\langle h^- \rangle$
W^2 (GeV^2)
(b) $W^2 < 10$ GeV
(c) $10 < W^2 < 20$ GeV
(d) $W^2 > 20$ GeV
Q^2 (GeV/c)^2

Figure 2

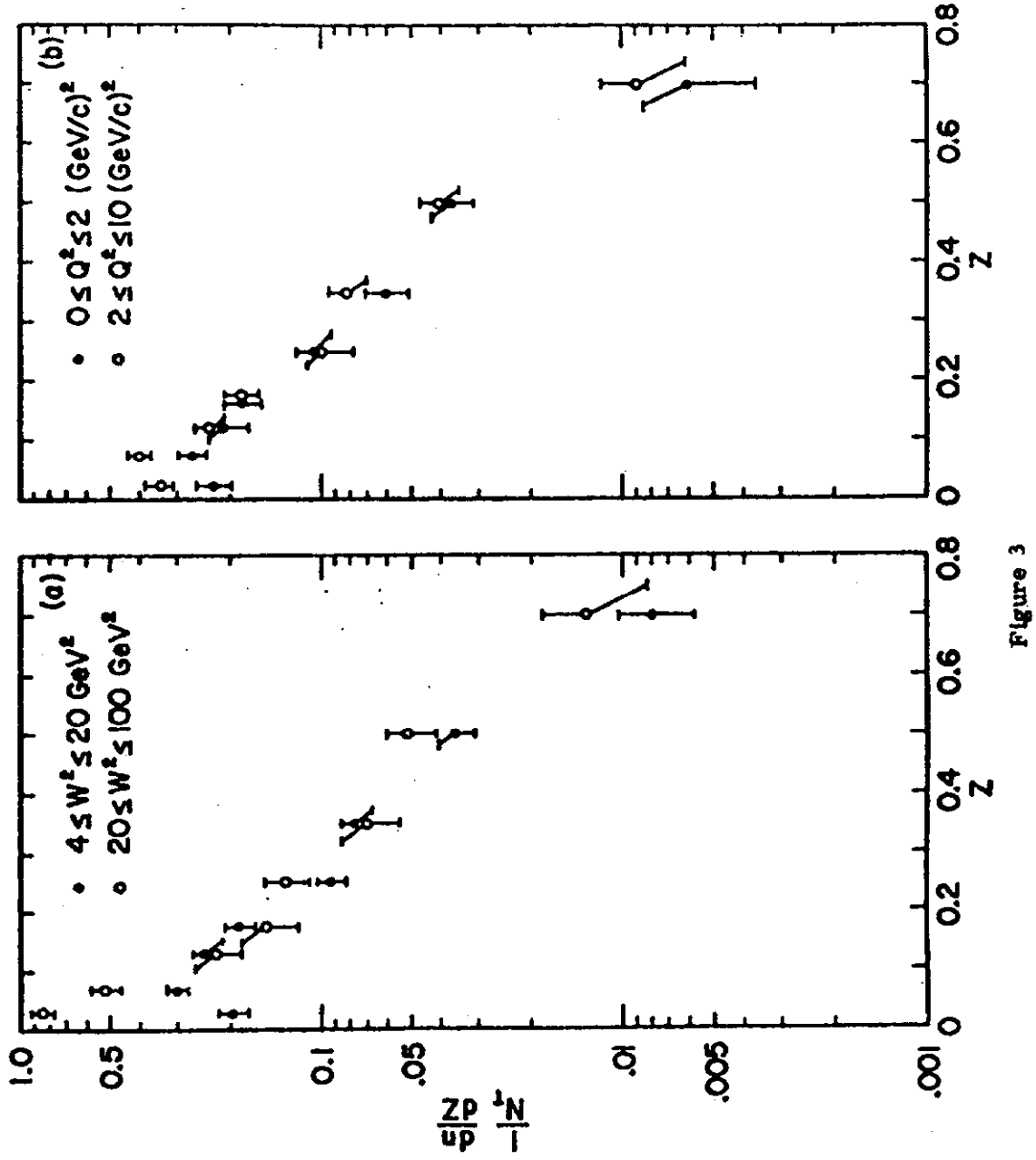
(a)
• 4≤W²≤20 GeV²
○ 20≤W²≤100 GeV²
(b)
• 0≤Q²≤2 (GeV/c)²
○ 2≤Q²≤10 (GeV/c)²
z
1.0
0.5
0.1
.05
.01
.005
.001
0
0.2
0.4
0.6
0.8
$\frac{1}{N}\frac{dn}{dz}$

Figure 3

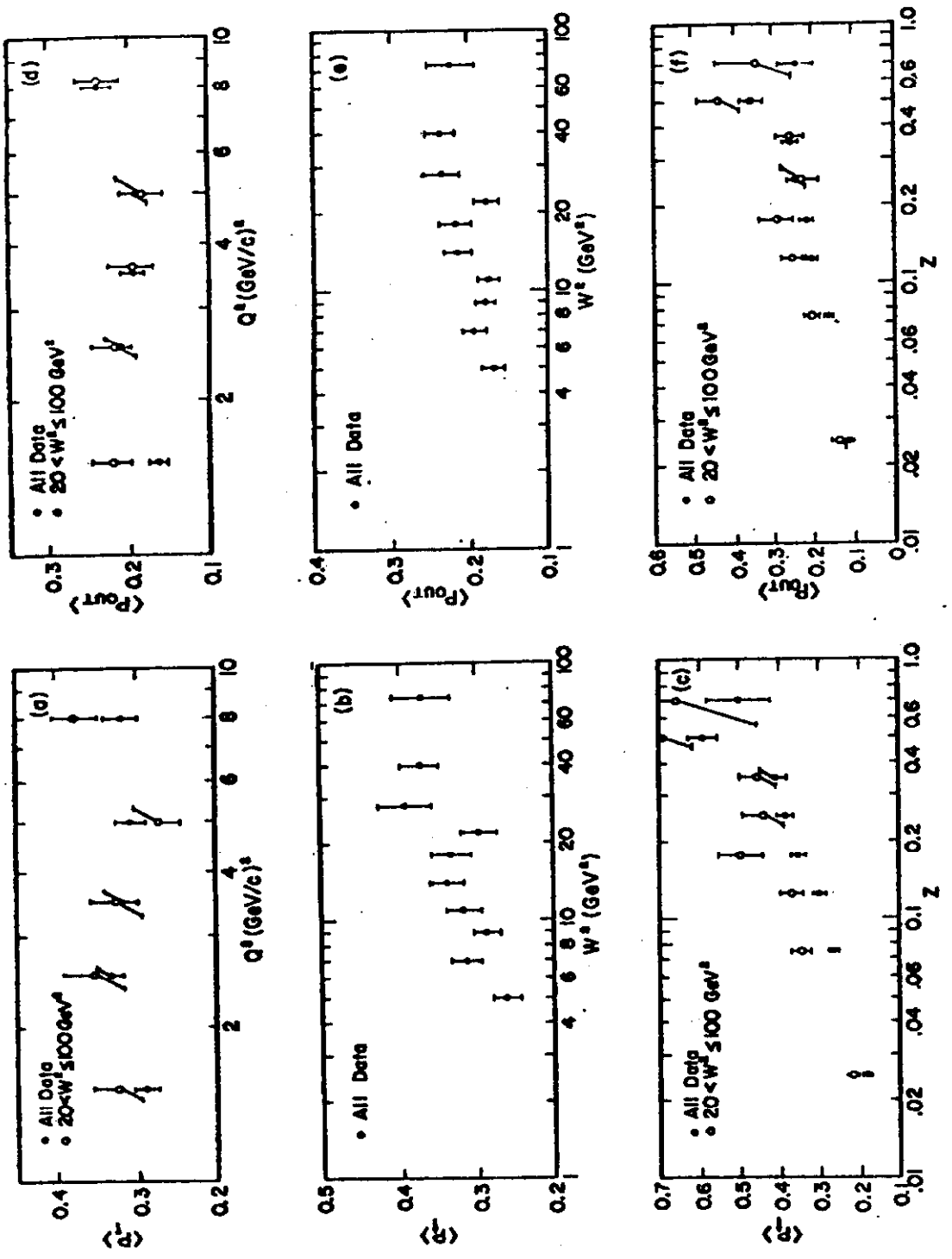
(a)
(b)
(c)
(d)
(e)
(f)
• All Data
• 20<W²≤100 GeV²
$\langle \frac{1}{d} \rangle$
$\langle P_{out} \rangle$
$\langle \frac{R}{d} \rangle$
$\langle R_{out} \rangle$
Q^2 (GeV/c)²
W^2 (GeV²)
z

Figure 4

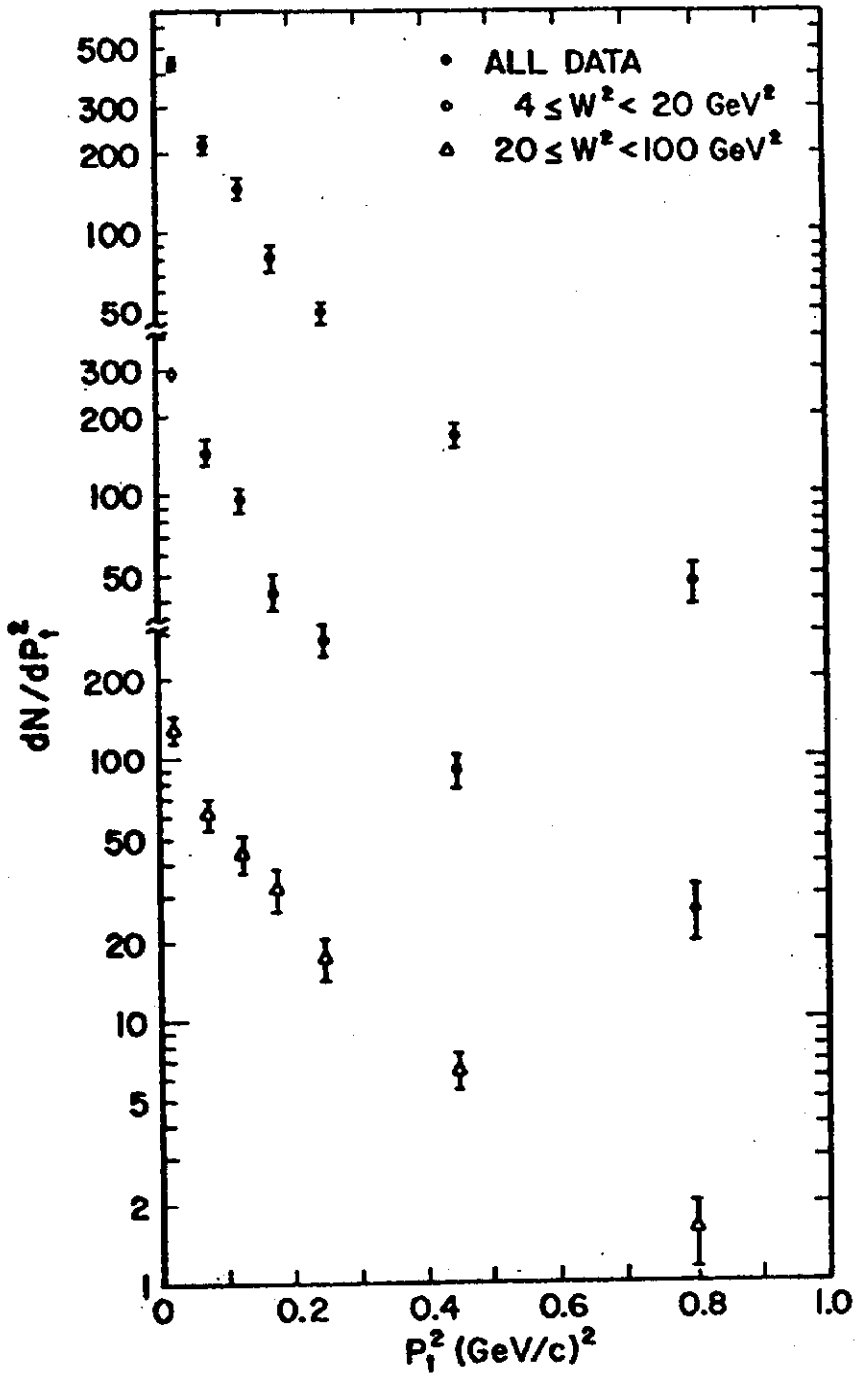
ALL DATA
4 ≤ W² < 20 GeV²
20 ≤ W² < 100 GeV²
dN/dP₁²
P₁² (GeV/c)²
500
300
200
100
50
300
200
100
50
200
100
50
20
10
5
2
1
0
0.2
0.4
0.6
0.8
1.0

Figure 5

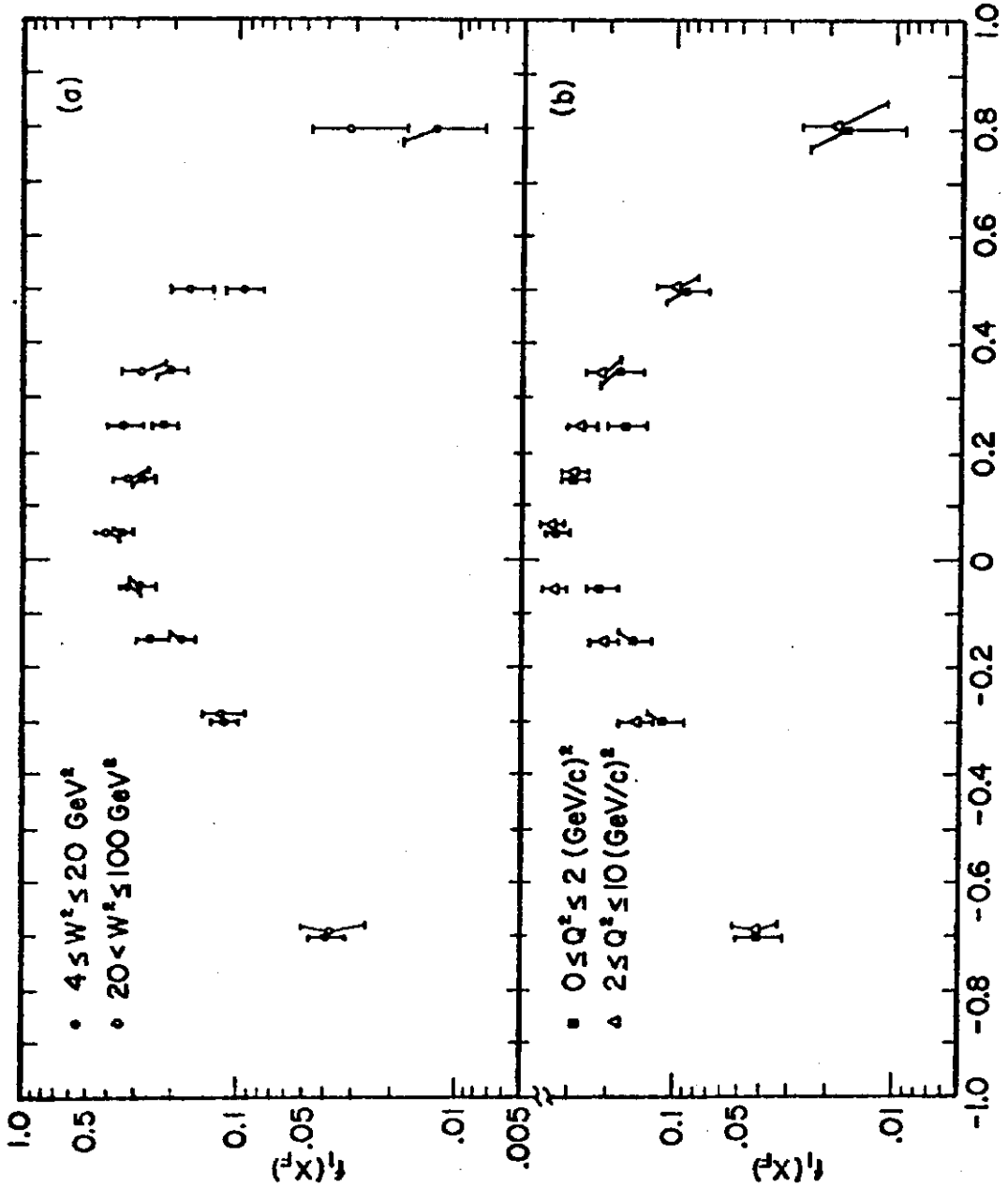
(a)
(b)
• 4≤W²≤20 GeV²
○ 20<W²≤100 GeV²
■ 0≤Q²≤2 (GeV/c)²
▲ 2≤Q²≤10 (GeV/c)²
f₁(x_F)
x_F
1.0
0.5
0.1
.05
.01
.005
-1.0
-0.8
-0.6
-0.4
-0.2
0
0.2
0.4
0.6
0.8
1.0

Figure 6

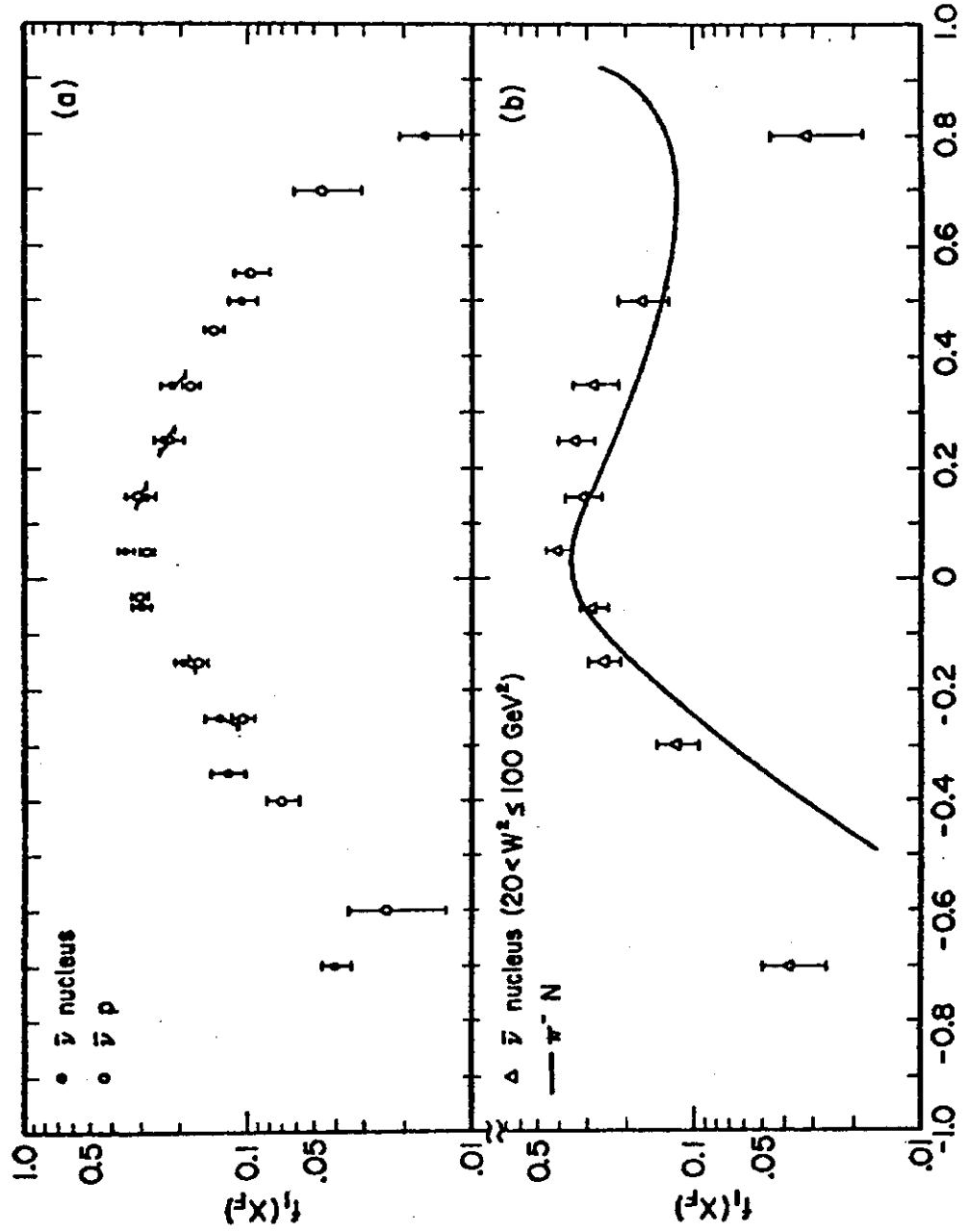
(a)
• $\bar{\nu}$ nucleus
○ $\bar{\nu}$ p
(b)
▲ $\bar{\nu}$ nucleus (20<W²≤100 GeV²)
— π⁻ N
$f_1(x_F)$
x_F
1.0
0.5
0.1
.05
.01
-1.0
-0.8
-0.6
-0.4
-0.2
0
0.2
0.4
0.6
0.8
1.0

Figure 7